Use of global sensitivity analysis and polynomial chaos expansion for interpretation of nonreactive transport experiments in laboratory-scale porous media

Noura Fajraoui,[1] Fanilo Ramasomanana,[1] Anis Younes,[1] Thierry Alex Mara,[2] Philippe Ackerer,[1] and Alberto Guadagnini[3]

Received 8 June 2010; revised 8 October 2010; accepted 22 October 2010; published 15 February 2011.

[1] In this work, we show how the use of global sensitivity analysis (GSA) in conjunction with the polynomial chaos expansion (PCE) methodology can provide relevant information for the interpretation of transport experiments in laboratory-scale heterogeneous porous media. We perform GSA by calculating the Sobol indices, which provide a variance-based importance measure of the effects of uncertain parameters on the output of a chosen interpretive transport model. The choice of PCE has the following two benefits: (1) it provides the global sensitivity indices in a straightforward manner, and (2) PCE can serve as a surrogate model for the calibration of parameters. The coefficients of the PCE are computed by probabilistic collocation. The methodology is applied to two nonreactive transport experiments available in the literature, while considering both transient and pseudo steady state transport regimes. This method allows a rigorous investigation of the relative effects and importance of different uncertain quantities, which include boundary conditions as well as porous medium hydraulic and dispersive parameters. The parameters that are most relevant to depicting the system's behavior can then be evaluated. In addition, one can assess the space-time distribution of measurement points, which is the most influential factor for the identifiability of parameters. Our work indicates that these methods can be valuable tools in the proper design of model-based transport experiments.

Citation: Fajraoui, N., F. Ramasomanana, A. Younes, T. A. Mara, P. Ackerer, and A. Guadagnini (2011), Use of global sensitivity analysis and polynomial chaos expansion for interpretation of nonreactive transport experiments in laboratory-scale porous media, *Water Resour. Res., 47*, W02521, doi:10.1029/2010WR009639.

1. Introduction

[2] Laboratory-scale flow cells are commonly used to examine the interplay between processes affecting solute transport through porous media under controlled conditions. One advantage of flow cells is their suitability for relatively fast and reliable experiments. Measuring the spatial distributions of a state variable (i.e., the solutes' concentrations) within the cell is often difficult. Generally, fluid is sampled only at the flow cell outlet or at a set of predefined locations within the system. In this context, colorimetric techniques based on high-resolution image analysis are becoming increasingly popular [e.g., *Gramling et al.*, 2002; *Cirpka et al.*, 2006; *Oates and Harvey*, 2006; *Konz et al.*, 2009a, 2009b] as they allow the obtainment of the complete map of the space-time evolution of solute concentrations for certain types of porous media and substances.

[3] Interpretations of transport experiments are typically performed on the basis of models based on, for example, the advection-dispersion equation (ADE), multirate mass transfer concepts, or the continuous time random walk framework [e.g., *Berkowitz et al.*, 2006, and references therein]. Regardless of the underlying complexity, the key parameters of the model adopted are calibrated against the observed state variable at (space-time) locations which are chosen during the design phase of the experiment.

[4] Several sources of uncertainty need to be quantified and controlled in order to obtain a data set that allows the key features of the observed processes during a model-based interpretive phase to be understood. These features typically include boundary conditions (e.g., the fluid flow-rate adopted in the experiment), the spatial distribution of the hydraulic parameters of the system (i.e., the hydraulic conductivity and porosity of the materials used to fill the flow cell), and transport-related parameters (e.g., dispersivities when an ADE-based model is employed).

[5] The number of parameters associated with conservative transport laboratory experiments is not as large as in field-scale applications, which involve complex and highly heterogeneous systems. A simple and robust analysis technique can then be used to detect sensitivities and interactions between parameters. A rigorous global sensitivity analysis has been shown to provide high-quality information for

[1]Laboratoire d'Hydrologie et de Géochimie de Strasbourg, Université de Strasbourg, EOST, CNRS, Strasbourg, France.
[2]Department de Physique, PIMENT, Université de La Réunion, Moufia, La Réunion.
[3]Dipartimento di Ingegneria Idraulica, Ambientale, Infrastrutture Viarie e Rilevamento, Politecnico di Milano, Milan, Italy.

Copyright 2011 by the American Geophysical Union.
0043-1397/11/2010WR009639

identifying the main parameters controlling the variability of a model's output, and for serving as an effective precursor to optimal experiment design. The methodology has found applications in the assessment of laboratory experiments in system biology [e.g., *Kontoravdi et al.*, 2005; *van Riel*, 2006; *Kiparissides et al.*, 2009, and references therein], reliability engineering [e.g., *Frey and Patil*, 2002; *Marrel et al.*, 2009], and within practices of risk assessment of groundwater pollution [e.g., *Volkova et al.*, 2008].

[6] Here we use variance-based sensitivity indices [*Sobol*, 1993, 2001; *Homma and Saltelli*, 1996] for the global sensitivity analysis (GSA) of an ADE-based model of nonreactive transport in laboratory-scale reconstructed heterogeneous porous media. Variance-based sensitivity indices are known to be good descriptors of the sensitivity of the model to its inputs because they do not rely on any assumptions regarding the linearity or monotonous behavior of the model [*Saltelli et al.*, 2006]. However, depending on the sampling scheme adopted, the computation of these indices might require a large number of model evaluations. This situation can be unacceptable for time-consuming transport computer codes, on the basis of which parameter calibration is also performed, according to the results of the sensitivity analysis. Here we present the use of a general methodology for sensitivity analysis and parameter estimation that can be adopted in this context. The method we present includes the extraction of a surrogate model that mimics the main characteristics of the complete process model selected.

[7] Among different alternatives, we explore the use of polynomial chaos expansion (PCE) for depicting conservative transport experiments. The PCE is derived from the process model itself, and it typically allows the required sensitivity indices to be estimated with acceptable computational time and accuracy. The polynomial chaos theory was originally developed by *Wiener* [1938], and it has been extensively used in various engineering fields [e.g., *Ghanem and Spanos*, 1991; *Xiu and Karniadakis*, 2003; *Acharjee and Zabaras*, 2007]. The PCE has been used for uncertainty or risk analysis of flow in saturated [*Li and Zhang*, 2007] and unsaturated zones [*Li et al.*, 2009], and for multiphase flow [*Li and Zhang*, 2009].

[8] One of the key advantages of building a surrogate model with PCE is that it allows for computation of the variance-based indices analytically via a simple postprocessing of the PCE coefficients [*Sudret*, 2008]. Therefore, the computational cost of the complete set of sensitivity indices is reduced to that of estimating the PCE coefficients. We show in this work how the use of the GSA method in conjunction with the PCE technique can provide valuable information in the analysis of two laboratory experiments involving the transport of nonreactive solutes in heterogeneous flow cells. The results are assessed in terms of the potential of the methodology to provide (1) relevant parameters and their region of influence; (2) guidance in a model-based design of transport experiments in laboratory-scale porous media; and (3) a surrogate model for parameter calibration.

2. Overview of the Experiments and Data Sets

[9] We focus on the transport experiments presented by *Katz et al.* [2010] and *Konz et al.* [2009a, 2009b]. In both cases, the movement of a nonreactive solute is monitored within a flow cell where a block-heterogeneity is reconstructed by packing the system with two different materials. The flow conditions are steady state and spatially nonuniform in both cases. While the experiment of *Katz et al.* [2010] is focused on pseudo steady state transport conditions, that of *Konz et al.* [2009a, 2009b] aims at depicting the transient features of transport. As such, the experiments are characterized by different sets of controlling parameters and potential design strategies of the space-time collocation of sampling points. The salient features of the experiments are presented in the following.

[10] The experimental setup described by *Katz et al.* [2010] consisted of a 25 cm $\times$ 10 cm laboratory flow cell filled with porous media, saturated with an initial aqueous solution of sodium chloride. The packing of the cell was performed by embedding a trapezoidal-shaped region filled with sand material (average grain size of 0.532 mm; estimated average permeability $K_0 = 1.47 \times 10^{-10}$ m^2; estimated average porosity of 0.32) within a background matrix constituted by 1-mm glass beads (measured porosity of 0.375; estimated permeability $K_0 = 1.12 \times 10^{-9}$ m^2). The inlet face was split crosswise to create two separate inlets, side-by-side, each with a length of 5 cm. A 5 mm diameter hole was placed approximately in the middle of the outlet face, to create strongly nonuniform flow conditions. The structure of the flow cell and the setup for the experiments are illustrated in Figure 1.

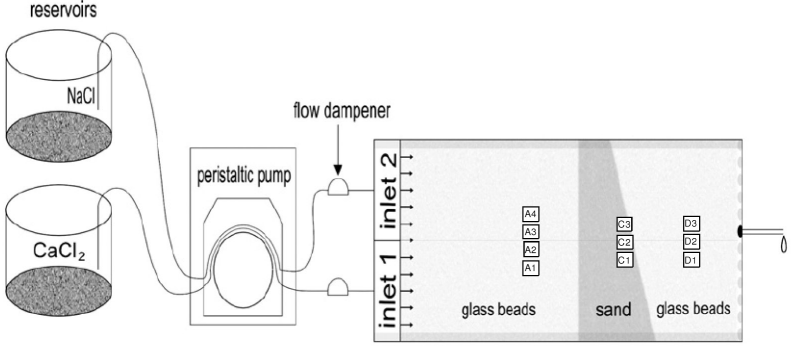

Figure 1. Sketch of the experimental setup adopted by *Katz et al.* [2010], including the locations of measurement ports.

[11] Calcium chloride and the initial sodium chloride solutions entered the cell through inlets 1 and 2 of Figure 1, respectively. Ten sampling ports were created on the top face of the cell. Their location is shown in Figure 1. BD microfine syringes were used to sample water from the inside of the flow cell through the ports. The calcium concentration was then measured in the samples. The analytical measurement error (a Cary 100 UV-vis spectrophotometer was used) was considered to be negligible relative to the scale of the concentrations detected in the experiment. Repeatability was investigated in the context of the experiments. The measurements collected were representative of pseudo steady state transport conditions. Additional details regarding the preparation of the solutions, the duration of the experiment, and the sampling and measuring techniques are reported by *Katz et al.* [2010].

[12] *Katz et al.* [2010] interpreted the transport experiments on the basis of the ADE model, using the code Retraso Code Bright (RCB) [*Saaltink et al.*, 2004]. According to the observed pseudo steady state conditions, the authors considered the transverse dispersivities of the glass beads and sand materials to be the only calibration parameters. These parameters were estimated by a best fit of the numerical simulations against concentrations measured at the ports within the cell during the experiments. During the calibration procedure, a ratio of 2:1 was maintained between the dispersivities of the glass beads and the sand, respectively. Due to limitations in the code, the authors could not use a very fine grid discretization, and they obtained transverse dispersivities of 0.8 mm and 0.4 mm, respectively, for the glass beads and the sand. These dispersivity values were deemed suitable to provide an adequate overall interpretation of the observed data.

[13] The setup described by *Konz et al.* [2009a] consisted of an experimental flow tank of 158 cm × 98 cm × 4 cm constructed of Plexiglas panes. This tank facilitated the optical observation of dyed plumes. Figure 2 displays a sketch of the experimental system. Two glass beads types (SiLi-beads GmbH) were used to pack the heterogeneous porous system. The diameters of the fine and coarse beads were 0.6 mm and 2 mm, respectively. The photometrical concentration measurement method was described by *Konz et al.* [2009b]. Time-lapse photography was applied to monitor the progress of the experiments using a digital camera (Nikon D70). A red food dye (Cochineal Red A, E124) marked the contaminant. The intensity distribution of the dye was converted to concentrations using a nonlinear relation of reflected intensity and dye concentration. This relationship was determined for each image pixel specifically by calibration experiments, and it was described by a second-order exponential function. The measurement error was estimated to be about 1% for the measured intensities [*Konz et al.*, 2009b].

[14] A flow from the lower left side to the lower right side was induced in the experiment. A constant flow rate (mean value 29.0 cm^2/min per unit thickness) was imposed by means of a peristaltic pump.

[15] The hydraulic parameters of the coarse and fine beads were determined in situ in the flow tank using pressure and flow measurements. Permeability values ranging between 2.6×10^{-10} and 4.0×10^{-10} m^2 were found for the fine beads zone. These values are consistent with those derived by *Konz et al.* [2009a], who provided an estimated permeability of 3.4×10^{-10} m^2 on the basis of a tracer experiment performed in a homogeneous medium packed with the same beads. Permeabilities ranging between 25×10^{-10} and 40×10^{-10} m^2 were found for the coarse beads zone. The Kozeny-Carman equation also suggested these values of permeability for the coarse beads zone to be 1 order of magnitude larger than those of the fine beads zone. The porosity was determined as 0.375 for both zones on the basis of volumetric and gravimetric measurements. The reader is referred to *Konz et al.* [2009a, 2009b] for additional details. The boundaries of the low-permeability block were digitized to accurately describe the geometrical pattern of the interface between the fine beads block and the high-permeability zone.

3. Polynomial Chaos Expansion for Sensitivity Analysis

3.1. Variance-Based Sensitivity Indices

[16] Let us consider a mathematical model associated with the M-independent random parameters $\boldsymbol{\zeta} = \{\zeta_1, \zeta_2, \ldots, \zeta_M\}$ that leads to a random response $f(\boldsymbol{\zeta})$ at a given space-time location. *Sobol* [1993] showed that if $f(\boldsymbol{\zeta})$ belongs to the space of square integrable functions, L_2, then it can be expanded as

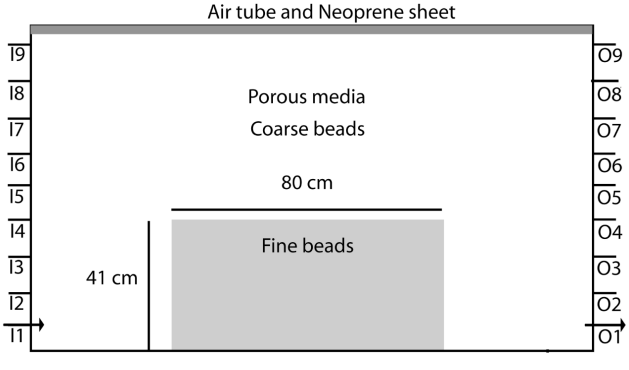

Figure 2. Experimental setup with boundary conditions adopted by *Konz et al.* [2009a, 2009b]. Arrows indicate the inflow and outflow sections.

$$f(\boldsymbol{\zeta}) = f_0 + \sum_{i=1}^{M} f_i(\zeta_i) + \sum_{j>1}^{M} f_{ij}(\zeta_i, \zeta_j) + \cdots + f_{1\ldots M}(\zeta_1, \ldots, \zeta_M), \quad (1)$$

where f_0 is the expected value of $f(\boldsymbol{\zeta})$, and $f_{i_1,\ldots,i_s}$ ($\{i_1,\ldots,i_s\} \subseteq \{1,\ldots,M\}$) are orthogonal functions. This representation is typically denoted analysis of variance (ANOVA) decomposition. Indeed, squaring (1) and taking the expectation leads to the variance decomposition of $f(\boldsymbol{\zeta})$,

$$V = \sum_{i=1}^{M} V_i + \sum_{j>1}^{M} V_{ij} + \cdots + V_{1\cdots M}, \quad (2)$$

where V denotes the total variance of $f(\boldsymbol{\zeta})$, V_i is the partial variance due to the input ζ_i alone, and $V_{i_1,\ldots,i_s}$ is the partial variance due to the interactions of the inputs belonging to the parameters' subset $\{\zeta_{i_1}, \ldots, \zeta_{i_s}\}$. The variance-based sensitivity indices of Sobol are then defined by

$$S_{i_1\ldots i_s} = \frac{V_{i_1\ldots i_s}}{V}. \quad (3)$$

[17] The sensitivity indices measure the contribution of an input to the output variance either solely or by interactions with the other inputs. One can define 2^M-1 sensitivity indices from (2). The first-order sensitivity index (also named the main effect of ζ_i) is defined by

$$S_i = \frac{V_i}{V}, \quad (4)$$

and it measures the expected amount by which the variance of $f(\boldsymbol{\zeta})$ is reduced when the true value of ζ_i is known and is associated with the identifiability of the parameter ζ_i, i.e., a high value of S_i (i.e., $S_i \approx 1$) indicates that the parameter ζ_i can be accurately estimated. In this work, all of the sensitivity indices are calculated by means of the polynomial chaos expansion (PCE) technique with a nonintrusive sampling strategy.

3.2. Polynomial Chaos Expansion

[18] We start by noting that any square integral random response admits the following chaos representation [*Soize and Ghanem*, 2004],

$$f(\boldsymbol{\zeta}) = \sum_{\alpha\in\mathbb{N}^M} s_\alpha \Psi_\alpha(\boldsymbol{\zeta}) = s_o\psi_0 + \sum_{i=1}^{M} s_i\psi_1(\zeta_i) + \sum_{j\geq i}^{M} s_{ij}\psi_2(\zeta_i,\zeta_j) + \sum_{k\geq j}^{M} s_{ijk}\psi_3(\zeta_i,\zeta_j,\zeta_k) + \ldots \quad (5)$$

where ψ_α is a αth-order multivariate orthogonal polynomial, $\boldsymbol{\zeta}$ is the input vector formed by M-independent and identically distributed random variables, and the $S_{i_1,\ldots,i_s}$'s are the polynomial coefficients. The orthogonal polynomial family depends on the joint probability distribution function of $\boldsymbol{\zeta}$ [e.g., *Xiu and Karniadakis*, 2002]. Because of the orthogonality of the polynomials, (5) is an ANOVA decomposition similar to (1). Thus, PCE can be seen as an approximation of the summands in (1) by orthogonal polynomials. For computational purposes, the series in (5) is truncated to polynomials of degree not exceeding p,

$$f(\boldsymbol{\zeta}) \approx \sum_{|\alpha|\leq p} s_\alpha \Psi_\alpha(\boldsymbol{\zeta}), \quad (6)$$

where $|\alpha| = \sum_{i=1}^{M} \alpha_i$ and the number of polynomial coefficients is $N_p = (M+p)!/(M!p!)$. The computation of the Sobol indices is straightforward once the vector of polynomial chaos coefficients $\boldsymbol{S} = [s_0, s_1, \ldots, s_P]^T$ are known. The sampling strategy adopted to compute $\boldsymbol{S}$ is discussed in section 3.3.

3.3. Probabilistic Collocation

[19] There are several nonintrusive computational approaches to computing the polynomial chaos (PC) coefficients. The term nonintrusive indicates that the PC coefficients are investigated through several evaluations of the function of interest by sampling the input values (the collocation points). For example, one can employ Monte Carlo or quasi-Monte Carlo sampling. It has been shown [*Sudret*, 2008; *Zhang et al.*, 2010] that probabilistic collocation methods perform better, in terms of convergence property, especially when M is small (i.e., less than 8).

[20] Let us assume that an M-variate Hermite polynomial of degree p is investigated. One can rewrite the truncated PC expansion using vector notation as

$$f(\boldsymbol{\zeta}) = \boldsymbol{\Psi}(\boldsymbol{\zeta})\mathbf{S}. \quad (7)$$

[21] Probabilistic collocation assigns the values of the roots of monodimensional Hermite polynomials of degree $(p+1)$ to each input [*Tatang et al.*, 1997]. The size of the full sampling design, then, is $(p+1)^M$. As a consequence, one has to select a number $N \geq N_p$ of collocation points among all possible combinations so that the information matrix $\boldsymbol{A} = (\boldsymbol{\Psi}^T\boldsymbol{\Psi})$ defined by

$$A_{ij} = \sum_{k=1}^{N} \psi_i(\zeta^k)\,\psi_j(\zeta^k) \quad (8)$$

is invertible and well-conditioned. We denote by $\boldsymbol{F}$ the vector of function evaluations at the different collocation points, that is, $F_k = f\left(\boldsymbol{\zeta}^{(k)}\right)$ $(k = 1, \ldots, N)$, where $\boldsymbol{\zeta}^{(k)}$ is the kth collocation point. The PC coefficients can then be computed by least squares regression as

$$S = \left(\boldsymbol{\Psi}^T\boldsymbol{\Psi}\right)^{-1}\boldsymbol{\Psi}^T\mathbf{F}. \quad (9)$$

[22] Regression-based methods often select the collocation points closest to the origin of the sampling space [*Huang et al.*, 2007; *Li and Zhang*, 2007; *Sudret* 2008]. We note that the minimal sample size is $N = N_p$. Since setting $N = N_p$ may lead to an ill-conditioned matrix, an algorithm based on singular value decomposition should be used. In this work, we use the technique suggested by *Sudret* [2008], which alleviates the problem of having an ill-conditioned matrix but requires a sample size $N > N_p$.

4. Modeling Procedure

[23] The experiments described in section 2 are modeled by means of a standard ADE. Very fine meshes (around

17,000 elements for the first experiment and 30,000 for the second) are used. Because several simulations are required, an efficient and accurate simulator for the solution of the ADE is needed. Moreover, the analyzed transport experiments are advection dominated, so that standard Eulerian methods such as finite elements or finite differences are not well-suited for the modeling task because these may generate solutions with artificial diffusion and/or unphysical oscillations. In this work, we solve the ADE by means of the Eulerian-Lagrangian localized adjoint method (ELLAM) [*Younes and Ackerer*, 2005; *Younes et al.*, 2006]. This method can use large time steps because the advection term is approximated accurately without any Courant Friedrich Levy (CFL) restriction. The ELLAM formulation developed by *Younes et al.* [2006] for unstructured triangular meshes uses only strategic numerical integration points and, therefore, requires a limited number of integration points (usually one per element). To avoid numerical dispersion due to interpolation, when several time steps are used, the method uses a continuous tracking of characteristics, and only changes due to dispersion are interpolated at each time step. Note that accurate calculations of fluxes at element edges are required to track the particles. In this work, the flow equation is solved with the mixed finite element approximation detailed by *Younes et al.*, [2008]. With this formulation, the velocity is defined everywhere in the field, and its normal component is continuous across the interelement boundaries. Therefore, accurate analytical characteristic tracking can be obtained using the mixed velocity field.

[24] Sensitivity analysis of the random transport process is performed under conditions corresponding to those for which experimental data have been collected, i.e., pseudo steady state and transient transport for the experiments of *Katz et al.* [2010] and *Konz et al.* [2009a, 2009b], respectively. The flow is steady state in both cases. This approach allows, on the one hand, an assessment of the sampling choice performed by *Katz et al.* [2010] and, on the other hand, an extraction of measurements with high information content from the wide database of *Konz et al.* [2009a, 2009b].

4.1. Sensitivity Analysis of the Experiment of *Katz et al.* [2010]

[25] The experiment of *Katz et al.* [2010] is analyzed by considering that randomness of model outputs is associated with only four random input parameters, as described in the following. We set $Q_{\text{up}} = Q_0(1 + \varepsilon_Q)$ and $Q_{\text{low}} = Q_0(1 - \varepsilon_Q)$. Q_{up} and Q_{low} are the flow rates across inlets 1 and 2 of Figure 1, respectively, while 2 Q_0 is the total inlet flowrate provided by *Katz et al.* [2010]. In this sense, the random parameter ε_Q accounts for a nonuniform distribution of the inlet flow rate, 2 Q_0, between the upper and lower halves of the flow cell. We then define the average permeability of the sand region as $K^s = \varepsilon_K K_0^s$, K_0^s being the permeability value adopted by *Katz et al.* [2010]. Finally, we set the transverse dispersivities of the glass (α_T^b) and sand (α_T^s) materials to $\alpha_T^b = \varepsilon_\alpha^b \alpha_T^{b,0}$ and $\alpha_T^s = \varepsilon_\alpha^s \alpha_T^{s,0}$. Here ε_α^b and ε_α^s are random calibration parameters, and $\alpha_T^{b,0} = 0.2$ mm is the dispersivity value obtained by *Katz et al.* [2010] by means of a conservative transport experiment performed upon filling the cell with glass beads only. Following *Katz et al.* [2010], we then assume that $\alpha_T^{s,0} = \alpha_T^{b,0}/2$. For illustration purposes, and without loss of generality, we consider the initial and inlet solutes' concentrations, the average porosities of the two media, and the hydraulic conductivity of the glass beads' background matrix as deterministically given, and we set their values to those provided by *Katz et al.* [2010]. Longitudinal dispersivities are excluded from the set of random model parameters as the data of *Katz et al.* [2010] corresponds to pseudo steady state conditions.

[26] The range of variability of the random parameters considered is prescribed on the basis of considerations about the magnitude of the measurement/interpretation errors (for hydraulic conductivities and inlet flux) and the physically plausible intervals of the parameters' variability (for dispersivities). Therefore, we assume that $0 \le \varepsilon_Q \le 0.06$, $0.5 \le \varepsilon_K \le 2$, $0.5 \le \varepsilon_\alpha^b \le 2$, and $0.5 \le \varepsilon_\alpha^s \le 2$. A uniform distribution is assumed for each random parameter so that Legendre polynomials are employed for the PCE. The coefficients of the PCE are evaluated for all of the nodes of the mesh according to the methodology described in section 3.3.

[27] Figure 3 illustrates the spatial distribution of the mean normalized calcium concentrations obtained on the basis of a PCE of order $p = 4$ after 2 hours, from the beginning of the simulated experiments, when the pseudo steady state conditions were attained at all sampling ports (note that the total duration of the experiment reported by *Katz*

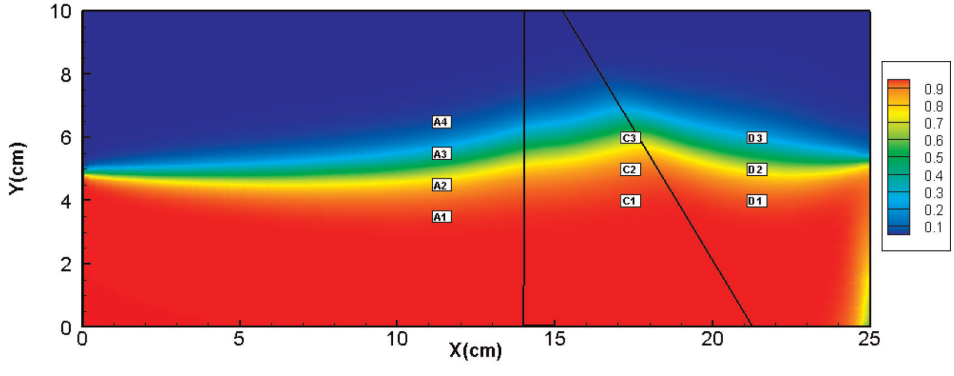

Figure 3. Spatial distribution of the pseudo-state mean normalized calcium concentrations obtained on the basis of a PCE of order $p = 4$ after 2 hours from the beginning of the experiment of *Katz et al.* [2010].

et al. [2010] is 4 hours). The corresponding depictions for the concentration variance are shown in Figure 4. These were obtained on the basis of PC sampling from 122 runs of the ADE, and they are considered sufficiently accurate in comparison with those obtained by means of 2500 numerical simulations of the ADE (not shown) performed by standard Monte Carlo sampling of the random parameters space. We note that pseudo steady state conditions were attained in the domain, with the sole exception of a small region corresponding to a stagnation area in the bottom right corner. This small region is located at some distance from all of the measurement ports, and it does not influence the sampled concentrations.

[28] The sensitivity of the concentration field to the variability of the random input parameters can be assessed by means of spatial maps of the Sobol indices. Inspection of the sensitivity indices showed that the interactions between the parameters chosen were not significant (not shown). Consequently, we focus on the parameters' main effects. Figure 5 shows the spatial distribution of the main effects due to uncertainty in (a) the inlet flux distribution, S_1; (b) the sand's average permeability, S_2; and (c) the transverse dispersivity of the glass beads' medium, S_3. As one should jointly assess the extent of the region where the parameters' sensitivity is significant and the spatial distribution of the global concentration variance, we juxtapose in Figure 5 the boundary of the region within which the coefficient of variation, CV, of the calculated normalized concentration is larger than 5%.

[29] The main effect due to the transverse dispersivity of the sand is not shown because its maximum calculated value inside the domain is less than 10^{-3}, implying that the concentration variance is not sensitive to α_T^s. This finding is likely associated with the short residence time of the solute within the sand inclusion. It follows that the transverse dispersivity of the sand is not an influential parameter for the experimental conditions analyzed, and within the selected range of variability, i.e., it could be set at any nominal value within the selected interval without producing any significant effect on the model output. Consequently, this parameter should not be used in an inverse modeling procedure based on this experimental setup, and the number of parameters to calibrate is reduced. This implies that the experimental design and the sampling scheme of *Katz et al.* [2010] are not conducive to a reliable estimate of α_T^s. We note that the interval of values we chose for constraining the variability of transverse dispersivity is consistent with the observation that dispersivity is correlated to grain size [*Dullien*, 1979].

[30] We also note that the results of the transport model are highly sensitive to the inlet flux distribution (embedded in the parameter ε_Q) at locations close to the upstream boundary and in the proximity of the locations of the flow lines associated with the 0.5 normalized average calcium concentrations. In contrast, the model has a very low sensitivity to the transverse dispersivity of the glass beads' medium at locations close to the flow line dividing the upper from the lower part of the cell. The sensitivity to this parameter increases with the distance from this region. This result is consistent with the physics embedded in the adopted process model based on the ADE.

[31] The effect of the sand's permeability is not confined solely within the low-permeability inclusion. It is seen to also extend upstream and downstream from the region packed with sand. This suggests that the calibration of K^s could benefit from pseudo steady state concentration data collected at points that are spread around the inclusion. Two areas are identified where a sensitivity to ε_K larger than 0.9 is calculated. One of these areas is mostly confined within the trapezoidal inclusion, while the other comprises a region close to the bottom corner of the flow cell downstream from the inclusion. The latter corresponds to a stagnation area in the system, the extent of which is mainly driven by the slope of the sand inclusion. This result highlights the power of an appropriate and robust model-driven experimental design. In this particular case, though, the values of CV are not negligible only in a limited portion of the domain within this sensitive area, which might complicate the installation of effective measuring ports within this region. We note that the detection of this sensitive region is associated with the concentration field failing to reach the pseudo steady state in this area for the simulation time considered.

[32] The assessment of the interactions among the parameters is computed in a straightforward manner upon relying on the PCE coefficients. We found small interactions between (1) ε_Q and ε_K, and (2) ε_K and ε_α^b. The interactions between ε_Q and ε_K are localized within areas of

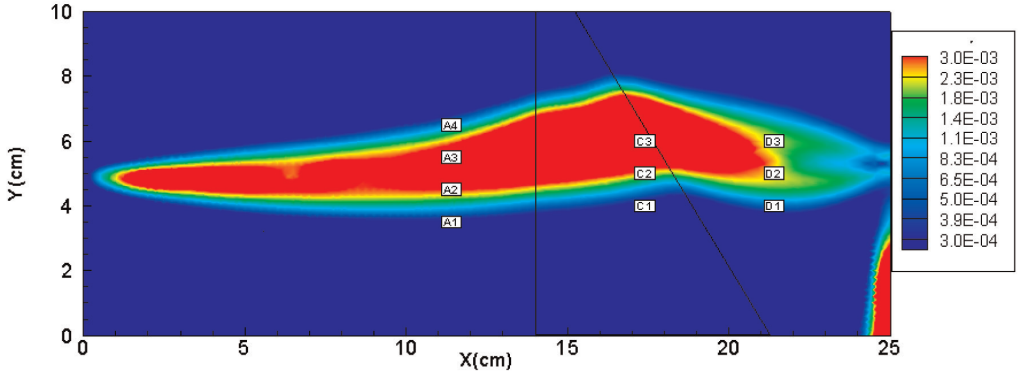

Figure 4. Spatial distribution of the variance of the normalized calcium concentrations obtained on the basis of a PCE of order $p = 4$, after 2 hours from the beginning of the experiment of *Katz et al.* [2010].

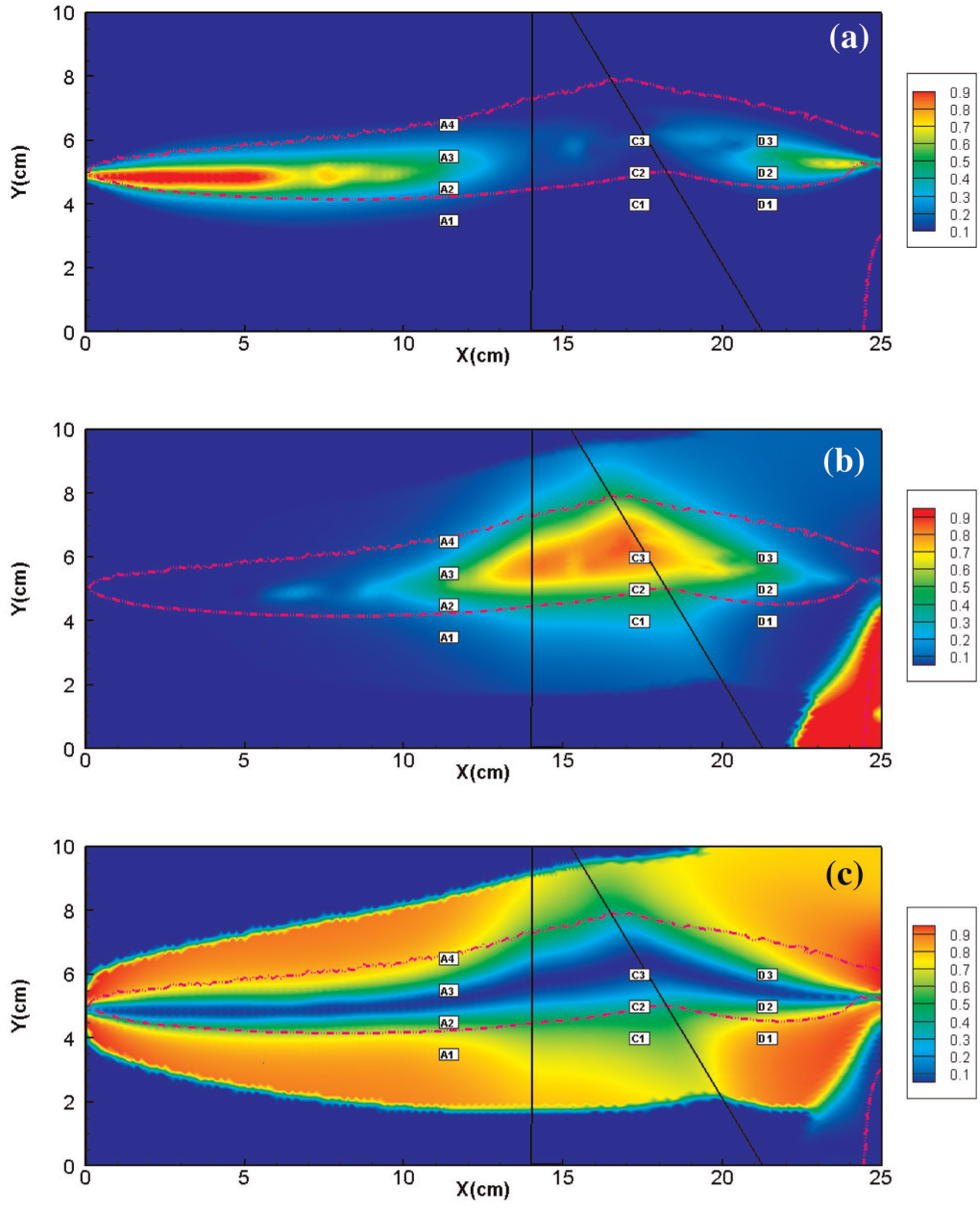

Figure 5. Spatial distribution for the experiment of *Katz et al.* [2010] of the main effects due to uncertainty in (a) the inlet flux distribution, S_1; (b) the sand average permeability, S_2; and (c) the transverse dispersivity of the glass beads medium, S_3. Dashed lines denote the boundary of the region within which the coefficient of variation, *CV*, of the calculated normalized concentration is larger than 5%.

large concentration variance. The opposite is noted for the interactions between ε_K and ε_α^b, suggesting that the experimental conditions adopted by *Katz et al.* [2010] are not influenced by this effect.

[33] The calibration of the most sensitive parameters can then be performed. We start by recalling that *Katz et al.* [2010] performed their calibration of the ADE by considering α_T^b as the only adjustable parameter, and they obtained significant differences between the experimental and simulated results at some of the measurement ports (their Figure 9). Here we perform an inverse modeling of the ADE, and we calibrate the inlet flux, K^s, and α_T^b (in terms of ε_Q, ε_K, and ε_α^b) within their interval of variation, while setting $\alpha_T^s = \alpha_T^b/2$, as in the work of *Katz et al.* [2010]. To this end, we use the genetic algorithm (GA) method [*Haupt and Haupt*, 2004]. The GA starts from an initial population, which is randomly generated within the range of variability of the parameters. The population then progresses throughout the generation process by using three genetic operators, i.e., (1) selection (determine the best individuals of the population); (2) crossover (combine two parents to generate two other individuals); and (3) mutation (modify an

individual to diversify the population) until convergence is reached. To evaluate the quality of the solution, we use the objective function

$$O = \frac{1}{N}\sqrt{\sum_{i=1}^{N}\left[w_i\left(C^i_{\text{mes}} - C^i_{\text{sim}}\right)\right]^2}. \quad (10)$$

[34] Here, C^i_{mes} and C^i_{sim} are the experimental and simulated pseudo steady state concentrations, respectively; N is the number of ports where the concentrations are measured, and w_i is the weight associated with C^i_{mes}. The values of the target concentrations C^i_{mes} are calculated as the average values of the concentrations measured during the pseudo steady state phase of the transport process at port i. The weight w_i is calculated as the inverse of the standard deviation of the pseudo steady state concentrations measured at port i and of the different replicates of the experiment.

[35] In this study, the simulated concentrations are obtained using the surrogate model, i.e., the PCE of order $p = 4$ presented in section 3 at the 10 measurement ports. We note that the PCE surrogate model is obtained for all of the nodes of the mesh using 122 runs of the ADE, as mentioned above. In this case, the convergence of the GA is obtained by means of 183 evaluations of the PCE, and it renders $O = 8.81 \times 10^{-5}$, requiring less than 1 s CPU time. The values of the calibrated parameters are $\varepsilon_Q = 0.058$, $\varepsilon_K = 1.57$ ($K^s = 2.31 \times 10^{-10}$ m^2), and $\varepsilon^b_\alpha = 0.7$ ($\alpha^b_T = 0.14$ mm). As a term of comparison, *Katz et al.* [2010] adopted $\varepsilon = 0$ and $K^s = 1.47 \times 10^{-10}$ m^2 (obtained from the application of the Kozeny-Carman equation on the basis of measured porosity and characteristic particle size measurements), and they manually calibrated α^b_T to a value of 0.8 mm. *Katz et al.* [2010] pointed out their inability to analyze values of $\alpha^b_T \leq 0.2$ mm, due to the lack of convergence of the numerical code.

[36] As an example of the quality of our results, Figure 6 shows the calibration results for ports A1, A2, D1, D2, and D3. We obtained results of similar quality (not shown) in terms of estimated concentrations and parameters by employing the GA sampling scheme in conjunction with the numerical solution of the ADE by ELLAM. In this case, 550 evaluations of the ADE model (to be compared against the 122 runs needed to obtain the PCE surrogate model for all nodes in the mesh) led to $O = 8.72 \times 10^{-5}$.

4.2. Sensitivity Analysis of the Experiment of *Konz et al.* [2009a, 2009b]

[37] We analyzed the experiment of *Konz et al.* [2009a, 2009b] by considering that the uncertainty of the model output is associated with six random input parameters: (1) the inlet flowrate, Q; (2) the average permeability of the region packed with coarse glass beads, K_{CB}; and (3) the longitudinal (α^j_L) and transverse (α^j_T) dispersivities of the two zones depicted in Figure 2 ($j = 1$ and 2 for the coarse and fine beads regions, respectively). The permeability value for the fine beads system, K_{FB}, is fixed to 3.4×10^{-10} m^2, which is an average value for this packing [*Konz et al.*, 2009a, 2009b]. This choice is based on the ratio K_{CB}/K_{FB} being the relevant factor for the given setup and boundary conditions. The sensitivity analysis was performed by constraining the parameters within the following ranges of variability: (1) $Q = Q_0(1 + \varepsilon_Q)$, with $Q_0 = 29$ cm^2/min and $-0.05 \leq \varepsilon_Q \leq 0.05$; $K_{CB} = \varepsilon_K K^0_{CB}$, with $K^0_{CB} = 25 \times 10^{-10}$ m^2 and $1 \leq \varepsilon_K \leq 1.6$; 1.0 mm $\leq \alpha^1_L \leq 10.0$ mm; 0.1 mm $\leq \alpha^1_L \leq 0.6$ mm; 0.3 mm $\leq \alpha^2_L \leq 3.0$ mm; and 0.03 mm $\leq \alpha^2_T \leq 0.3$ mm. Similar to the procedure we adopted in section 4.1, the ranges of variability were chosen on the basis of the works of *Konz et al.* [2009a, 2009b] and according to physical considerations about the nature of the parameters selected.

[38] The flow was considered to be steady state. A transport experiment of 288 min was simulated by using 240 time steps with a regular time interval of $\Delta t = 1.2$ min. A PCE of the order $p = 4$, requiring 478 runs of the transport model, allowed us to obtain sufficiently accurate results, i.e., no significant differences were detected by comparison against a PCE of order $p = 5$. Note that in this case, a PCE needs to be constructed for each node of the mesh and at each time step.

[39] As an example of the type of results obtained, Figure 7a depicts the spatial distribution of the mean dye concentration in the system after 120 min from the beginning of the simulation. The corresponding depiction of the distribution of the concentration variance due to the randomness

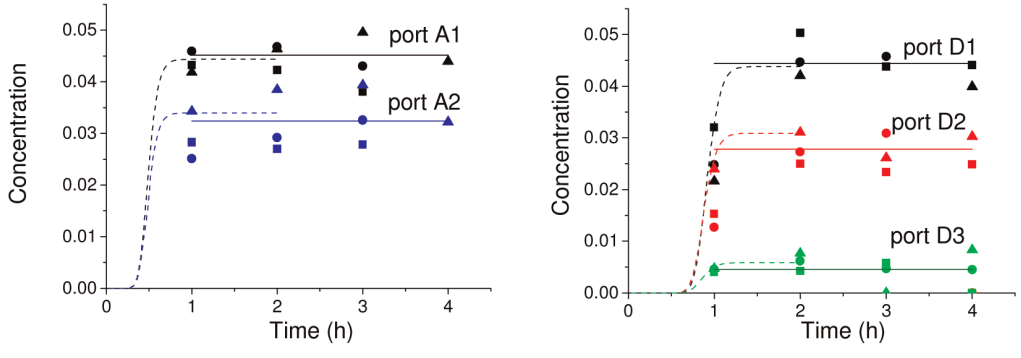

Figure 6. Calibration results for ports A1, A2, D1, D2, and D3 of *Katz et al.* [2010]; the symbols represent measurements performed during different replicates of the experiment; the dashed curves and solid lines correspond, respectively, to our simulation results and the experimentally based pseudo steady state concentrations at the ports.

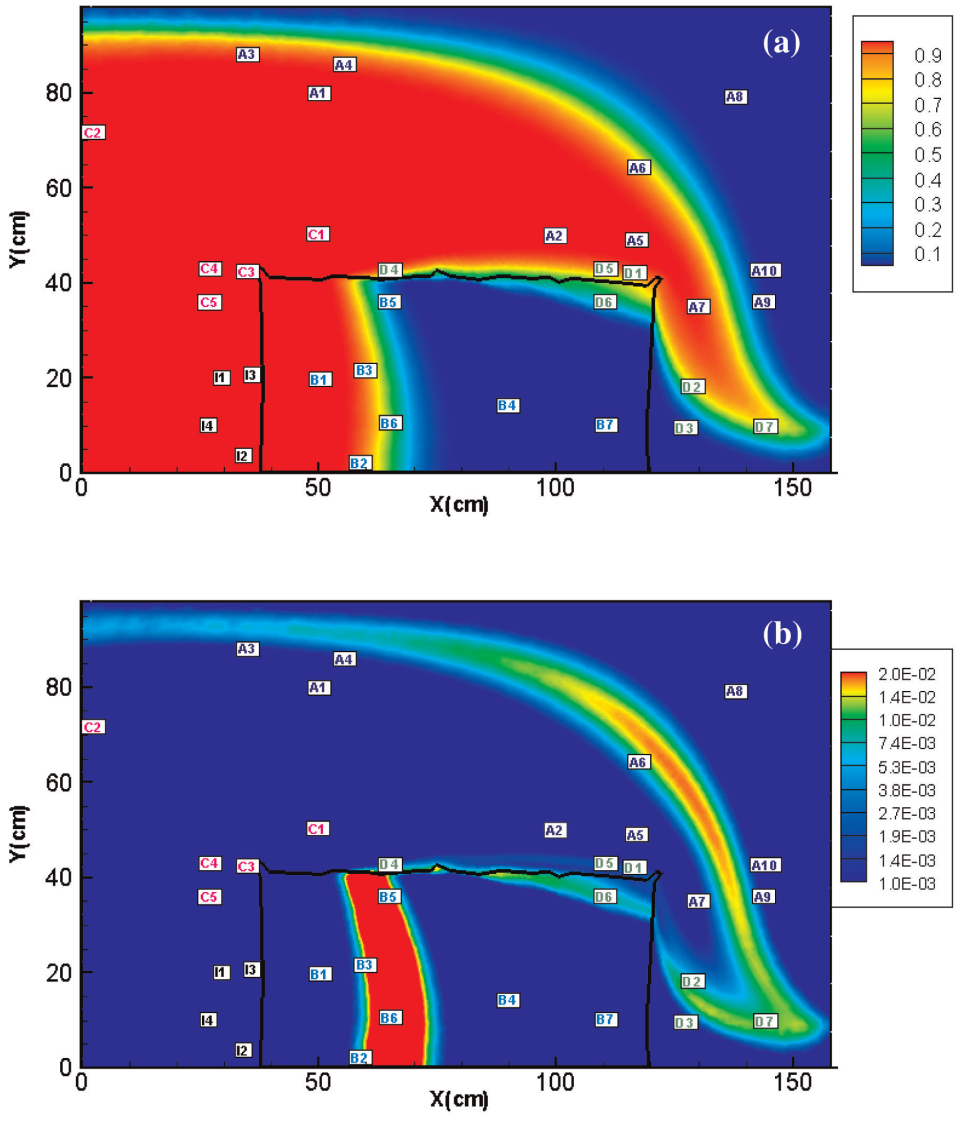

Figure 7. Spatial distribution of the (a) mean and (b) variance of the dye concentration in the system after 120 min from the beginning of the simulation of the experiment of *Konz et al.* [2009a, 2009b]. Sampling locations identified as A1–A10, B1–B7, C1–C5, D1–D7, and I1–I4 are representative of the different groups of sampling locations and are characterized by the different relative importance of the contributions of the random input parameters to the total concentration variance.

of input parameters is presented in Figure 7b. As a general comment, we note that the concentration variance is nonnegligible at locations close to the front of the advancing tracer. The largest variance values are mainly found around the solute advancing front within the low-permeability region. Based on the results of the sensitivity analysis, the sampling points can be classified into five groups. Each of these groups are characterized by a different and clearly distinguishable behavior in terms of the relative strength of the contributions of the random input parameters to the total concentration variance. Therefore, we present in detail the results of the sensitivity analysis only for a few selected points, which we consider as representative of the above-mentioned groups. Figure 7 depicts some of these sampling locations, which we have identified with the symbols A1–A10, B1–B7, C1–C5, D1–D7, and I1–I4, according to the grouping scheme we adopted. The parameter calibration was then performed upon selecting only a few of the sampling points reported in Figure 7.

[40] Figures 8–12 show examples of the temporal distribution of the concentration variance at selected representative sampling locations together with the relative contributions associated with the chosen random input parameters. The shaded area under the variance curve includes the partial marginal contributions of the random input parameters as well as the contribution of their interactions. An inspection of the results reveals that the occurrence of the variance peak at a given location depends on the travel time of the advancing front of the solute. The temporal distributions of the observed variances, including their values, depend on the observation point, consistent with the migration processes embedded in the numerical transport model adopted. At locations close to

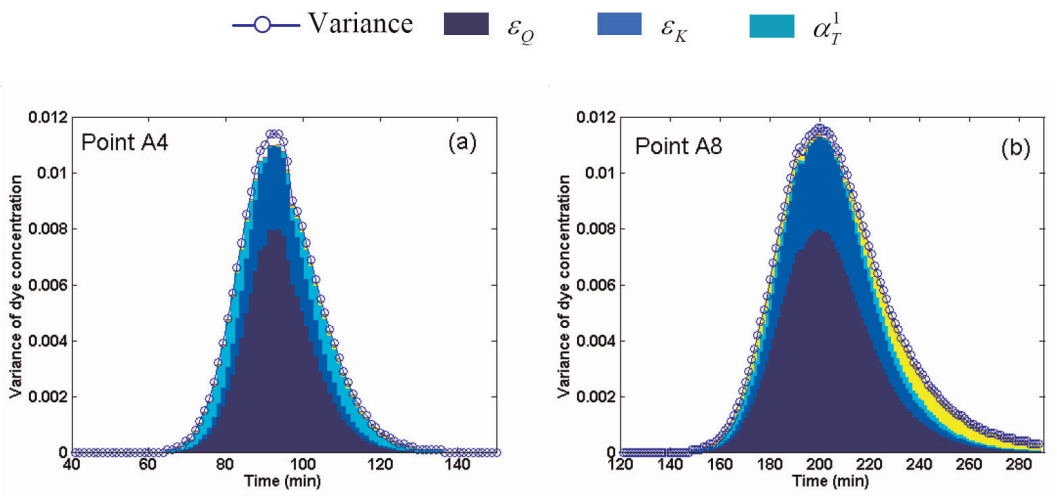

Figure 8. Time distribution of the concentration variance at selected sampling locations belonging to group A of the observation points (see Figure 7). The shaded area under the variance curve represents the partial marginal contributions of the random input parameters; the contribution of interactions between parameters is included in the blank region between the shaded area and the variance curve.

the upper interface between the two conductivity regions, a double peak of concentration variance can occur (see also Figure 11, sampling point D4). This occurrence is mainly related to the differential diffusion/dispersion of the solute between the two regions filled with different glass beads and to the effect of the advective component due to its proximity to the outlet section.

[41] As seen in Figure 8, the concentration variance at points located well inside the coarse beads region and in the upper half of the cell (group A of sampling points) is mainly driven by uncertainties in the inlet flux, Q, and, to some extent, K_{CB}. Of the remaining parameters, only the longitudinal dispersivity α_L^1 has some additional impact, depending on the location of the detection point in the system.

[42] A different behavior is associated with the sampling points located within the low-conductivity inclusion and belonging to group B (Figure 9). Here the concentration variance is chiefly governed by the contrast between the hydraulic conductivities of the two regions, which is consistent with the physics of the process. Only a very limited contribution is provided by Q, while the remaining parameters do not play any role in the process.

[43] The sensitivity to the transverse dispersivity, α_T^1, of the highly conductive region is largest in the region where the sampling points belonging to group C of Figure 7 are

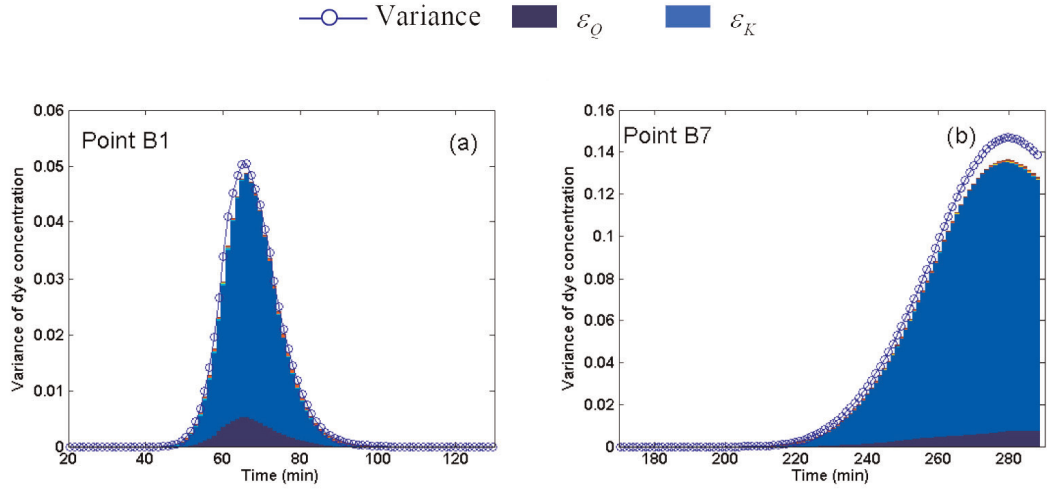

Figure 9. Time distribution of the concentration variance at selected sampling locations belonging to group B of the observation points in the experiment of *Konz et al.* [2009a, 2009b] (see Figure 7). The shaded area under the variance curve represents the partial marginal contributions of the random input parameters; the contribution of interactions between parameters is included in the blank region between the shaded area and the variance curve.

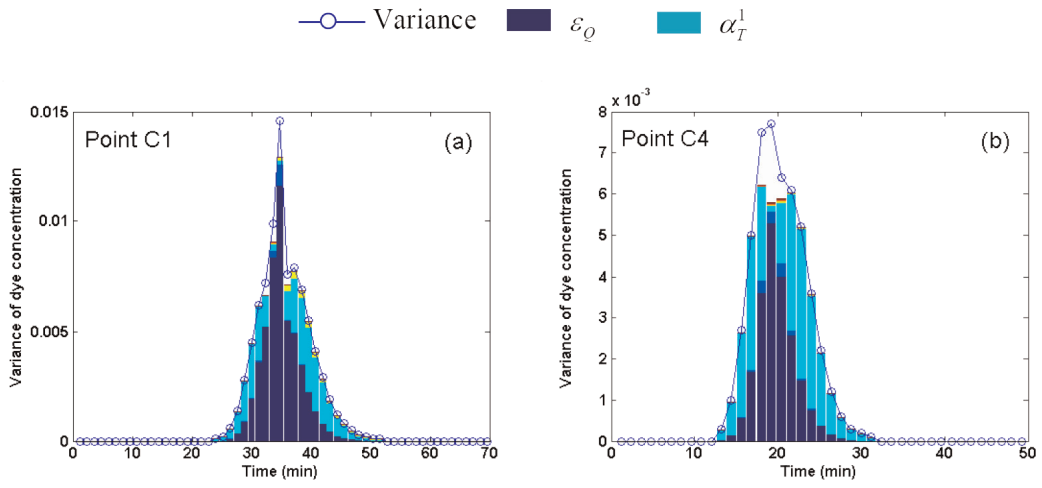

Figure 10. Time distribution of the concentration variance at selected sampling locations belonging to group C of the observation points in the experiment of *Konz et al.* [2009a, 2009b] (see Figure 7). The shaded area under the variance curve represents the partial marginal contributions of the random input parameters; the contribution of interactions between parameters is included in the blank region between the shaded area and the variance curve.

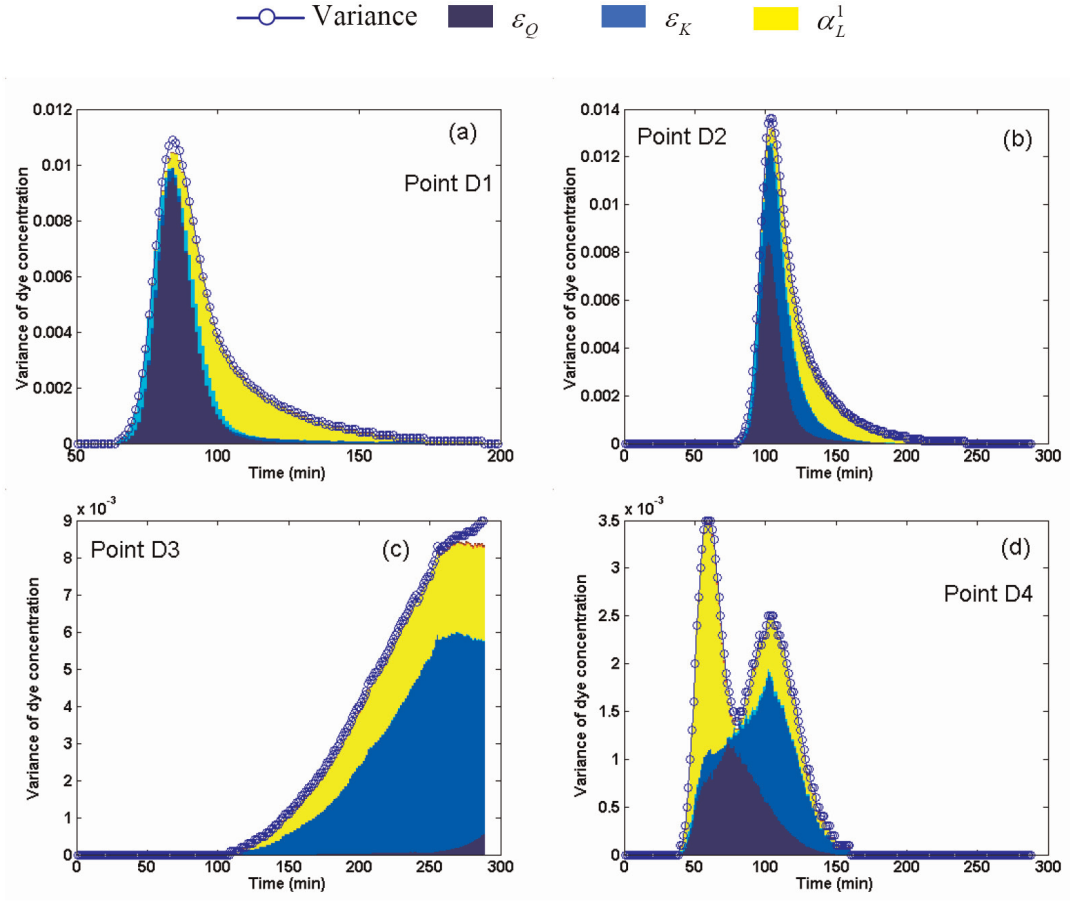

Figure 11. Time distribution of the concentration variance at selected sampling locations belonging to group D of the observation points in the experiment of *Konz et al.* [2009a, 2009b] (see Figure 7). The shaded area under the variance curve represents the partial marginal contributions of the random input parameters; the contribution of interactions between parameters is included in the blank region between the shaded area and the variance curve.

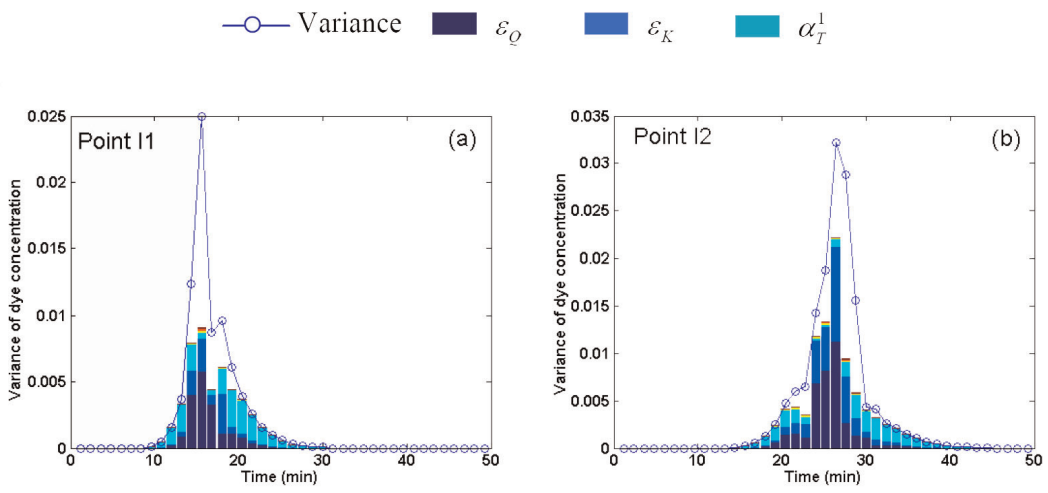

Figure 12. Time distribution of the concentration variance at selected sampling locations belonging to group I of the observation points in the experiment of *Konz et al.* [2009a, 2009b] (see Figure 7). The shaded area under the variance curve represents the partial marginal contributions of the random input parameters; the contribution of interactions between parameters is included in the blank region between the shaded area and the variance curve.

located. These locations are relatively close to the inlet, and significant sensitivities occur at relatively short observation times, consistent with the local displacement of the resident fluid. The other key controlling parameter in this area is Q, as the sampling points are located relatively close to the inlet section (Figure 10).

[44] The longitudinal dispersivity of the high conductivity region, α_L^1, has a relatively significant impact on the concentration variance at observation points located close to the horizontal interface between the high and low conductivity media, as well as in the low-velocity region downstream from the low-permeability inclusion. This result is detailed in Figure 11, where the results observed at selected points belonging to group D are reported. A contribution of Q can be detected at points relatively close to the inlet and outlet sections of the system (points D1, D4, and D2), while Q has a negligible effect at point D3 (Figure 11c), which is located in the low-velocity region downstream from the low-permeability inclusion. The effect of ε_K, representing the ratio between the permeabilities of the two subdomains, can be noted at some of these locations, and with various degrees of strength.

[45] Our results suggest that the concentration variance at the sampling points located upstream of the low-permeability inclusion and close to the bottom of the flow cell is strongly driven by interaction effects (Figure 12). These effects are mainly due to the combined effect of Q and K_{CB}. This behavior is opposite of that noted at all other locations in the system (Figures 8–11), where interactions are virtually absent or are associated with very low effects at all observation times.

[46] The analysis suggests that dye concentrations should be measured at points located within the four distinct regions identified as representative of the different sensitivities of the model response to the parameters. This approach allows the salient features of the system to be captured, and it is conducive to identifying the sensitive parameters during a calibration process. Finally, we note that our results indicate that the dispersivities of the low-permeability inclusion do not affect the solute pattern in the system, which suggests that the adopted experimental setup is not conducive to a reliable estimate of these parameters.

[47] We calibrate the model parameters on the basis of a few measurement points that insured that all of the identified groups of the sampling locations were represented. For demonstration purposes, we selected nine sampling points, i.e., A9, A10, B5, B6, C4, C5, D4, D5, and D6 (see Figure 7 for their location). The calibration was performed on the basis of the objective function reported in (10) upon setting N to the total number of time-varying concentration values (C^i_{mes}) measured at the above mentioned nine locations. The weights w_i were set to unity because only one replicate of the experiment was available for each observation time, and the measurement errors were the same at all points. The simulated concentrations were obtained using the surrogate model, i.e., the PCE of order $p = 4$ mentioned above. The parameters' space was searched by means of the same GA adopted in section 4.1. The convergence was attained with a CPU time of less than 4 s. The values of the calibrated parameters were $\varepsilon_Q = -1.9 \times 10^{-2}$ ($Q = 28.45$ cm^2/min), $\varepsilon_K = 1.25$ ($K_{CB} = 31.25 \times 10^{-10}$ m^2), $\alpha_L^1 = 0.15$ cm, and $\alpha_T^1 = 0.015$ cm. Note that on the basis of our results, the parameters to which the process is chiefly sensitive are only ε_Q and ε_K, while the system displays a moderate sensitivity to α_L^1 and α_T^1 (Figures 10 and 11). Consequently, the optimal values of α_L^2 and α_T^2 were not investigated in the calibration procedure.

[48] As an example of the quality of our results, Figure 13 shows the calibration results at points A9, D5, D6, B7, D7, and I4. Note that measurements at points B7, D7, and I4 were not used in the calibration procedure. It can be seen that the observed behavior of the system was reproduced to a high degree of accuracy by the calibrated model. Our results are consistent with those provided by *Konz et al.* [2009a, 2009b], who performed a preliminary sensitivity study by considering a few selected values of some of the indicated parameters.

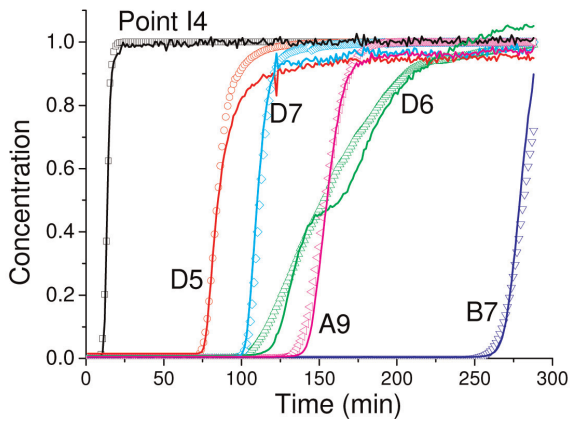

Figure 13. Calibration results for selected measurement points (see Figure 7 for their locations in the domain) in the experiment of *Konz et al.* [2009a, 2009b]; symbols and continuous lines represent computed and measured concentrations, respectively.

5. Conclusions

[49] Our work leads to the following key conclusions:

[50] 1. The use of global sensitivity analysis (GSA) based on the Sobol indices applied to a conservative transport model allows quantification of the influence of the model input parameters on the distribution of solute concentrations within a heterogeneous laboratory-scale porous medium. At the same time, adopting a surrogate model (or metamodel) to depict transport on the basis of the polynomial chaos expansion (PCE) theory allows a considerable reduction of the computation time required to predict the system response and is conducive to a straightforward estimation of the Sobol indices.

[51] 2. The methodology was employed to analyze two nonreactive transport experiments available in the literature. In both cases, and for demonstration purposes, we selected only a limited number of uncertain parameters. These parameters included quantities that can be affected by measurement uncertainty (e.g., model boundary conditions), and the hydraulic and dispersive parameters of the porous medium. The two experiments were associated with different transport regimes (pseudo steady state or transient) and with different information (measurement) availability. Our analysis allowed us to analyze in detail the sampling design adopted in one of the experiments. It has proved to be an effective tool for extracting space-time distributions of measurements with high information content from the wide database available in the other experiment analyzed.

[52] 3. The acquired knowledge of the input-output relationships provides valuable information for experiment design and characterization. This information can help with defining, for example, effective sampling or measurement planning, and with determining more precisely the values of sensitive parameters describing the system on the basis of the interpretive transport model adopted. Extending the methodology to deal with stochastic spatial distributions of flow (and possibly transport) parameters could be an interesting development in view of applications targeted toward risk analysis of large-scale contaminated aquifers and performance assessments of aquifer remediation schemes.

[53] **Acknowledgments.** This project was supported by CNRS and the Research Group GNR MoMaS (Modélisations Mathématiques et Simulations numériques liées aux problèmes de gestion des déchets nucléaires). Part of the work was developed while A. Guadagnini was "Professeur Invité" at the University of Strasbourg.

References

Acharjee, S., and N. Zabaras (2007), A non-intrusive stochastic Galerkin approach for modeling uncertainty propagation in deformation processes, *Comput. Struct.*, *85*, 244–254.

Berkowitz, B., A. Cortis, M. Dentz, and H. Scher (2006), Modeling non-Fickian transport in geological formations as a continuous time random walk, *Rev. Geophys.*, *44*, RG2003, doi:10.1029/2005RG000178.

Cirpka, O. A., A. Olsson, Q. Ju, M. D. A. Rahman, and P. Grathwohl (2006), Determination of transverse dispersion coefficients from reactive plume lengths, *Ground Water*, *44*, 212–221.

Dullien, F. A. L. (1979), *Porous Media: Fluid Transport and Pore Structure*, Academic, New York.

Frey, C. H., and S. R. Patil (2002), Identification and review of sensitivity analysis methods, *Risk Anal.*, *22*, 553–578.

Ghanem, R. G., and P. D. Spanos (1991), *Stochastic Finite Elements—A Spectral Approach*, Springer, Berlin.

Gramling, C, C. F. Harvey, and L. Meigs (2002), Reactive transport in porous media: A comparison of model prediction with laboratory visualization, *Environ. Sci. Technol.*, *36*, 2508–2514.

Haupt, R. L., and S. E. Haupt (2004), *Practical Genetic Algorithms*, 2nd ed., Wiley, New York.

Homma, T., and A. Saltelli (1996), Importance measures in global sensitivity analysis of nonlinear models, *Reliab. Eng. Syst. Safety*, *52*, 1–17.

Huang, S. P., S. Mahadevan, and R. Rebba (2007), Collocation-based stochastic finite element analysis for random field problems, *Probab. Eng. Mech.*, *22*, 194–205.

Katz, G. E., B. Berkowitz, A. Guadagnini, and M. W. Saaltink (2010), Experimental and modeling investigation of multicomponent reactive transport in porous media, *J. Contam. Hydrol.*, doi:10.1016/j.jconhyd.2009.11.002, in press.

Kiparissides, A., S. S. Kucherenko, A. Mantalaris, and E. N. Pistikopoulos (2009), Global sensitivity analysis challenges in biological systems modeling, *Ind. Eng. Chem. Res.*, *48*, 7168–7180.

Kontoravdi, C., S. P. Asprey, E. N. Pistikopoulos, and A. Mantalaris (2005), Application of global sensitivity analysis to determine goals for design of experiments: An example study on antibody-producing cell cultures, *Biotechnol. Prog.*, *21*, 1128–1135.

Konz, M., P. Ackerer, A. Younes, P. Huggenberger, and E. Zechner (2009a), Two-dimensional stable-layered laboratory-scale experiments for testing density-coupled flow models, *Water Resour. Res.*, *45*, W02404, doi:10.1029/2008WR007118.

Konz, M., P. Ackerer, P. Huggenberger, and C. Veit (2009b), Comparison of light transmission and reflection techniques to determine concentrations in flow tank experiments, *Exp. Fluids*, *47*, 85–93.

Li, H., and D. Zhang (2007), Probabilistic collocation method for flow in porous media: Comparisons with other stochastic methods, *Water Resour. Res.*, *43*, W09409, doi:10.1029/2006WR005673.

Li, H., and D. Zhang (2009), Efficient and accurate quantification of uncertainty for multiphase flow with probabilistic collocation method, *SPE J.*, *14*, 665–679, doi:10.2118/114802-PA.

Li, W., Z. Lu, and D. Zhang (2009), Stochastic analysis of unsaturated flow with probabilistic collocation method, *Water Resour. Res.*, *45*, W08425, doi:10.1029/2008WR007530.

Marrel, A., B. Iooss, B. laurent, and O. Roustant (2009), Calculations of Sobol indices for the Gaussian process metamodel, *Reliab. Eng. Syst. Safety*, *94*, 742–751.

Oates, P.M., and C. F. Harvey (2006), A colorimetric reaction to quantify fluid mixing, *Exp. Fluids*, *41*, 673–683.

Saaltink, M. W., F. Batlle, C. Ayora, J. Carrera, and S. Olivella (2004), RETRASO, a code for modeling reactive transport in saturated and unsaturated porous media, *Geol. Acta*, *2*(3), 235–251.

Saltelli, A., M. Ratto, S. Tarantola, and F. Campolongo (2006), Sensitivity analysis practices: Strategies for model-based inference, *Reliab. Eng. Syst. Safety*, *91*, 1109–1125.

Sobol, I. M. (1993), Sensitivity estimates for nonlinear mathematical models, *Math. Model. Comput.*, *1*, 407–414.

Sobol, I. M. (2001), Global sensitivity indices for nonlinear mathematical models and their Monte Carlo estimates, *Math. Comput. Simul.*, *55*, 271–280.

Soize, C., and R. Ghanem (2004), Physical systems with random uncertainties: Chaos representations with arbitrary probability measure, *SIAM J. Sci. Comput.*, *26*, 395–410.

Sudret, B. (2008), Global sensitivity analysis using polynomial chaos expansions, *Reliab. Eng. Syst. Safety*, *93*, 964–979.

Tatang, M. A., W. W. Pan, R. G. Prin, and G. J. McRae (1997), An efficient method for parametric uncertainty analysis of numerical geophysical models, *J. Geophys. Res.*, *102*, 21925–21932.

van Riel, N. A. W. (2006), Dynamic modelling and analysis of biochemical networks: Mechanism-based models and model-based experiments, *Brief. Bioinform.*, *7*, 364–374.

Volkova, E., B. Iooss, and F. Van Dorpe (2008), Global sensitivity analysis for a numerical model of radionuclide migration from the RRC "Kurchatov Institute" radwaste disposal site, *Stoch. Environ. Res. Risk Assess.*, *22*, 17–31.

Wiener, N. (1938), The homogeneous chaos, *Am. J. Math.*, *60*, 897–936.

Xiu, D., and G. E. Karniadakis (2002), The Weiner-Askey Polynomial Chaos for stochastic differential equations, *SIAM J. Sci. Comput.*, *24*(2), 619–644, doi:10.1137/S1064827501387826.

Xiu, D., and G. E. Karniadakis (2003), A new stochastic approach to transient heat conduction modeling with uncertainty, *Int. J. Heat Mass Transfer*, *46*, 4681–4693.

Younes, A., and P. Ackerer (2005), Solving the advection-diffusion equation with the Eulerian-Lagrangian localized adjoint method on unstructured meshes and non uniform time stepping, *J. Comput. Phys.*, *208*, 384–402.

Younes, A., P. Ackerer, and F. Lehman (2006), A new efficient Eulerian-Lagrangian localized adjoint method for solving the advection-dispersion equation on unstructured meshes, *Adv. Water. Resour.*, *29*, 1056–1074.

Younes, A., M. Fahs, and P. Ackerer (2008), A new approach to avoid excessive numerical diffusion in Eulerian-Lagrangian methods, *Comm. Numer. Methods Eng.*, *24*, 897–910.

Zhang, D., L. Shi, H. Chang, and J. Yang (2010), A comparative study of numerical approaches to risk assessment of contaminant transport, *Stoch. Environ. Res. Risk Assess.*, in press.

P. Ackerer, N. Fajraoui, F. Ramasomanana, and A. Younes, Laboratoire d'Hydrologie et de Géochimie de Strasbourg, Université de Strasbourg, EOST, CNRS, 1 rue Blessig, F-67084 Strasbourg, France.

A. Guadagnini, Dipartimento Ingegneria Idraulica, Ambientale, Infrastrutture Viarie, e Rilevamento, Politecnico di Milano, Piazza L. Da Vinci 32, I-20133 Milan, Italy. (alberto.guadagnini@polimi.it)

T. A. Mara, Department de Physique, PIMENT, Université de La Réunion, 15 Av. René Cassin, BP 7151, 97715 Moufia, La Réunion.